Cell Reports

M1 Intrinsically Photosensitive Retinal Ganglion Cells Integrate Rod and Melanopsin Inputs to Signal in Low Light

Graphical Abstract

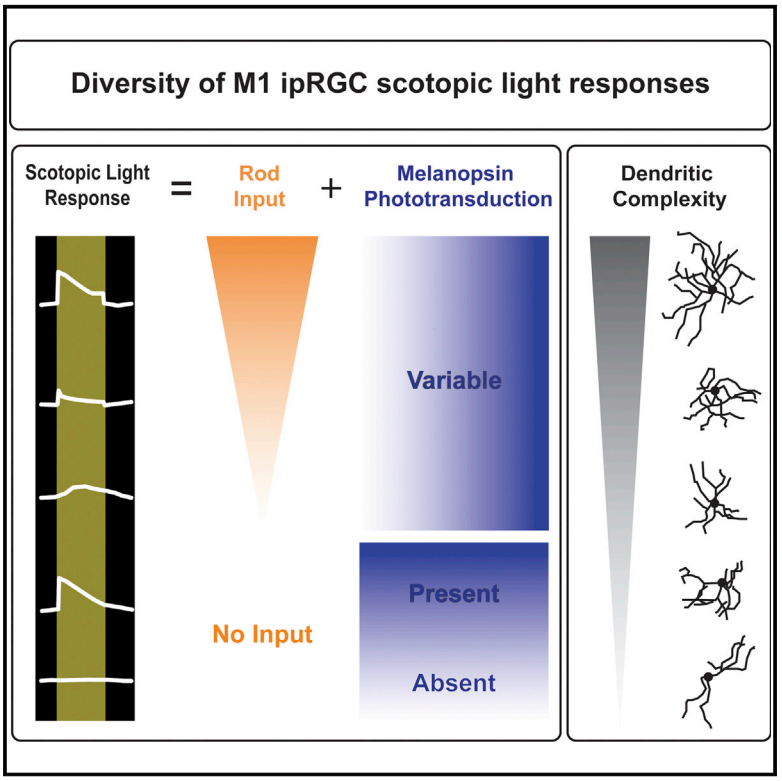

Highlights

- Low-light responses of M1 intrinsically photosensitive retinal ganglion cells (ipRGCs)
- M1 ipRGCs integrate melanopsin and rod signals at scotopic light intensities
- A subset of M1 ipRGCs show no response to scotopic light
- The strength of rod input correlates with morphological complexity of M1 ipRGCs

Authors

Seul Ki Lee, Takuma Sonoda, Tiffany M. Schmidt

Correspondence

tiffany.schmidt@northwestern.edu

In Brief

M1 intrinsically photosensitive retinal ganglion cells (ipRGCs) control an array of non-image-forming functions. Lee et al. report diverse light responses of M1 ipRGCs in scotopic light that are determined by the degree of rod and melanopsin inputs and find that degree of rod input correlates with dendritic complexity.

Lee et al., 2019, Cell Reports *29*, 3349–3355
December 10, 2019
https://doi.org/10.1016/j.celrep.2019.11.024

CellPress

Cell Reports
Report

M1 Intrinsically Photosensitive Retinal Ganglion Cells Integrate Rod and Melanopsin Inputs to Signal in Low Light

Seul Ki Lee,[1] Takuma Sonoda,[1] and Tiffany M. Schmidt[1,2,*]
[1]Department of Neurobiology, Northwestern University, Evanston, IL 60208, USA
[2]Lead Contact
*Correspondence: tiffany.schmidt@northwestern.edu
https://doi.org/10.1016/j.celrep.2019.11.024

SUMMARY

Light influences various behaviors and physiological processes that occur outside of our conscious perception, including circadian photoentrainment, sleep, and even learning and mood. The M1, melanopsin-expressing, intrinsically photosensitive retinal ganglion cells (ipRGCs) relay a combination of rod/cone and melanopsin signals to drive these functions. However, little is known about how M1 ipRGCs integrate these signals in low light. We measure the dim light response of M1 ipRGCs and find that they exhibit a wide spectrum of responses to dim, scotopic light stimulation that are driven by a combination of rod pathway input and melanopsin phototransduction. The presence of rod input to M1 ipRGCs correlates with larger and more complex dendritic arbors. Collectively, these results show variability in the rod input to M1 ipRGCs and a surprising contribution of melanopsin to the light responses of M1 ipRGCs at very low light.

INTRODUCTION

The non-image-forming visual system is responsible for mediating a range of light-driven processes, including circadian photoentrainment, the pupillary light reflex, masking, mood modulation, and hormonal regulation. These myriad functions are thought to be primarily mediated by the M1 subtype of melanopsin-expressing, intrinsically photosensitive retinal ganglion cells (ipRGCs), which directly project to more than 15 non-image-forming brain regions to execute these functions (Fernandez et al., 2016; Güler et al., 2008; Hattar et al., 2006; Li and Schmidt, 2018).

M1 ipRGCs are thought to rely heavily on rod signaling to mediate non-image-forming behaviors, because a lack of rod signaling results in major deficits in both pupil constriction and circadian photoentrainment (Altimus et al., 2010; Keenan et al., 2016). Therefore, understanding how rod signals are integrated by M1 ipRGCs is paramount for understanding how they mediate an array of non-image-forming functions. In dark-adapted tissue, M1 ipRGCs have been reported to receive synaptic input at light intensities as low as 7.5 log photons cm^{-2} s^{-1}, which is well into the scotopic range in which rod signaling predominates (Zhao et al., 2014). However, recent reports have also indicated that M1 ipRGCs vary widely across many other physiological and morphological properties (Emanuel et al., 2017). Despite the importance of rod input through M1 ipRGCs for light-driven behavior, it is unknown whether M1 ipRGCs exhibit similar variability in their processing of signals arising from the rod pathway.

Here, we systematically recorded from M1 ipRGCs in dark-adapted retinal tissue and report that most M1 ipRGCs (~88%) respond to dim, scotopic (7.5 log photons cm^{-2} s^{-1}) light. These responses were not uniform and consisted of a wide spectrum of response properties. Our results demonstrate that this diversity is generated by a combination of rod- and melanopsin-driven input and that there is a subset of M1 ipRGCs that receive little or no rod input, indicating that some M1 ipRGCs rely exclusively on melanopsin to signal dim light. In addition, we found that the strength of input from the rod pathway correlates with morphological complexity of M1 ipRGCs. Collectively, these data show a stark variability in the M1 ipRGC dim/scotopic light response driven by rod photoreceptors and melanopsin.

RESULTS

Diverse Responses of M1 ipRGCs to Dim/Scotopic Light

We first sought to characterize the properties of the M1 ipRGC dim light response. To do this, we recorded the light response of M1 ipRGCs to a dim (7.5 log photons cm^{-2} s^{-1}) light stimulation in *ex vivo* retinas of *Opn4-GFP* mice. We reasoned that this dim, scotopic light would allow us to assess the contribution of rod input to the M1 ipRGC light response. To maintain the cells in a dark-adapted state, we performed targeting of GFP-labeled ipRGCs with less than 10 s of 2-photon excitation (Figure S1A). M1 ipRGC identity was determined post hoc by confirming that dendrites stratified exclusively in the OFF sublamina (see STAR Methods). With this dim, scotopic light, most (29/42) M1 ipRGCs reached their maximum depolarization (max depolarization) within 5 s (called early-responding cells; Figures 1A and 1D), while 8/42 cells reached their maximum depolarizations after 5 s (called delayed-responding cells; Figures 1B and 1D) of light stimulation. Surprisingly, a subset of M1 ipRGCs (5/42) showed a lack of identifiable light response (called non-responding cells; Figures 1C and 1D), indicating that they receive no rod input. This lack of response was not due to poor retinal health in our recording conditions or bleached photoreceptors, because we were able to subsequently record dim light responses from

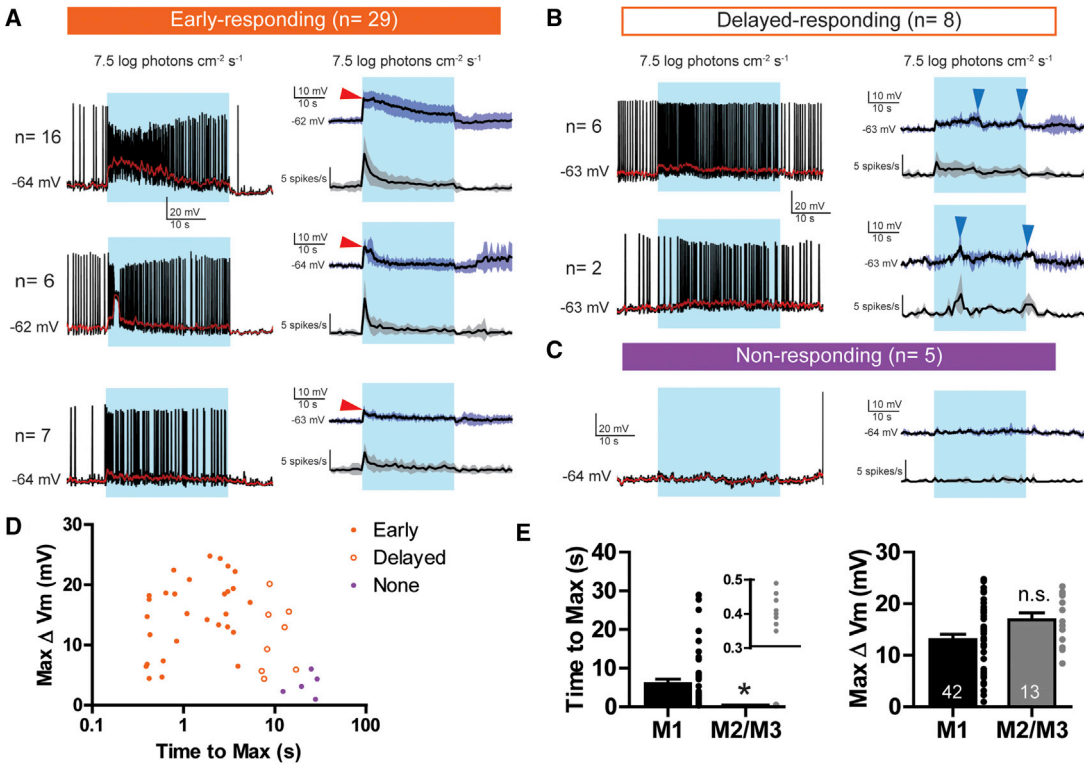

Figure 1. Diverse Responses of M1 ipRGCs to Dim/Scotopic Light

(A–C) Left panel shows representative voltage traces of early-responding (A), delayed-responding (B), and non-responding (C) M1 ipRGCs. Red lines indicate voltage traces filtered by a 0.5 s moving average. Right panel shows voltage trace averages (black) and SDs (blue shadow) and spike frequency (1 s bin) averages (black) and SDs (gray shadow). Red and blue arrows indicate maximum depolarization in the early and delayed responses, respectively.

(D) Scatterplot maximum depolarization (max Δ Vm) versus time to maximum depolarization (time to max, log scale) of M1 ipRGCs. Cells reaching their maximum depolarization at or before 5 s are classified as early-responding (closed orange circles, n = 29) M1 ipRGCs. Cells reaching their maximum depolarization after 5 s are classified as delayed-responding (open orange circles, n = 8) M1 ipRGCs. Cells lacking an identifiable light response are classified as non-responding (closed purple circles, n = 5) M1 ipRGCs. See also Figure S2.

(E) Left, time to reach maximum depolarization for M1 (coefficient of variation = 1.28; black) versus M2/M3 (coefficient of variation = 0.10; gray) ipRGCs. The inset shows an expanded view for time to max of M2/M3 ipRGCs over 0.3–0.5 s following light onset. Right, max Δ Vm of M1 (coefficient of variation = 0.52; black) and M2/M3 (coefficient of variation = 0.29; gray) ipRGCs. M1 ipRGCs show significantly longer time to max, similar max Δ Vm compared with M2/M3 ipRGCs. Bar graphs are mean ± SEM, *p < 0.05, unpaired t test.

neighboring ipRGCs (n = 4/4 cells tested; Figure S2A). In addition, in the M1 ipRGCs responding to scotopic light, we observed great variation in the size of dim light-evoked responses, with early-responding cells showing rapid onset but varying adaptation kinetics throughout the duration of the light stimulus (Figure 1A) while delayed-responding cells showed either rapid onset of the light response but delay in reaching the max depolarization (Figure 1B, top) or slow kinetics at light onset (Figure 1B, bottom). This variability was not due to photobleaching or adaptational changes, because M1 ipRGCs show consistent responses across multiple light stimulations (Figure S2B). The max depolarization versus the time to reach max depolarization is plotted for each M1 cell in Figure 1D and highlights the broad spectrum of size and kinetics in the M1 ipRGC response at this low light intensity. Overall, the time to max depolarization was significantly greater for M1 ipRGCs than for M2/M3 ipRGCs (time to max: 5.98 ± 1.18 s, n = 42 for M1, 0.40 ± 0.01 s, n = 13 for M2/M3, *p < 0.05, unpaired t test; Figure 1E) and more variable (coefficient of variation: 1.28 for M1, 0.10 for M2/M3; Figure 1E, left), though they did not differ in the magnitude of their depolarizations (max depolarization: 13.02 ± 1.05 mV, n = 42 for M1, 16.89 ± 1.36 mV, n = 13 for M2/M3, p = 0.06, unpaired t test; coefficient of variation: 0.52 for M1, 0.29 for M2/M3; Figure 1E, right). Therefore, the dim light response of M1 ipRGCs exhibits greater variability than that of other ipRGC subtypes.

Dim/Scotopic Light-Evoked Responses of M1 ipRGCs Are Driven by a Combination of Rod and Melanopsin Input

The lowest reported thresholds for melanopsin signaling in behavior or single-cell recordings are in the high scotopic or low mesopic range (i.e., ≥9 log photons cm^{-2} s^{-1}) (Berson et al., 2002; Ecker et al., 2010; Lucas et al., 2003; Milner and Do, 2017; Panda et al., 2003; Schmidt and Kofuji, 2009; Sonoda et al., 2018; Zhao et al., 2014). We therefore reasoned that the light response of M1 ipRGCs at 7.5 log photons cm^{-2} s^{-1} is driven primarily by rod signaling pathways. If this is the case, then the M1 ipRGC light response should be abolished following

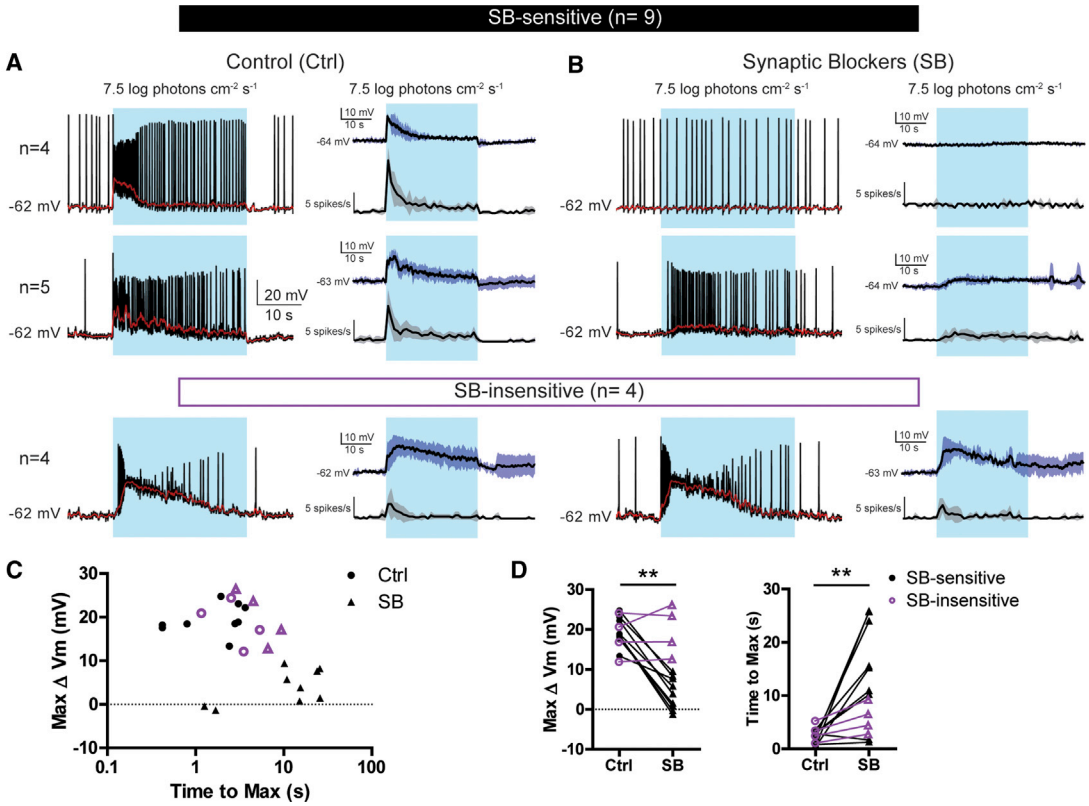

Figure 2. Dim/Scotopic Light-Evoked Responses of M1 ipRGCs Are Driven by a Combination of Synaptic and Melanopsin Input

(A and B) Scotopic light responses of M1 ipRGCs in control (Ctrl) solution (A) and synaptic blocker (SB) cocktail solution (B). Left panel shows representative voltage traces. Red lines indicate voltage traces filtered by a 0.5 s moving average. Right panel shows voltage trace averages (black) and SDs (blue shadow) and spike frequency (1 s bin) averages (black) and SDs (gray shadow). The light-evoked response of M1 ipRGCs is eliminated (top) or reduced (middle). The response of 4 cells (bottom) is unaffected by a blockage of synaptic inputs (SB-insensitive cells, indicated by open purple data points in C and D for visibility), indicating that the response is driven almost exclusively by melanopsin.

(C) Scatterplot of max Δ Vm versus time to max (log scale) of M1 ipRGCs in Ctrl (circles) and SB (triangles).

(D) Comparison of max Δ Vm (left) and time to max (right) of M1 ipRGCs between Ctrl and SB. Bar graphs are mean ± SEM, **$p < 0.005$, paired t test. The 4 cells showing no change in max Δ Vm highlighted in purple were included in the statistical analyses.

See also Figure S3.

application of synaptic blockers. To test this, we recorded dim light responses of M1 ipRGCs in the presence of a cocktail of synaptic blockers to silence synaptic input to M1 ipRGCs. Consistent with our prediction, we found that M1 ipRGCs exhibiting a dim light response showed a significant decrease in that light-evoked depolarization and a significant increase in time to max response following synaptic blocker application (Figures 2A–2D; max depolarization: 19.20 ± 1.07 mV for control [Ctrl], 8.87 ± 2.49 mV for synaptic blockers [SB], n = 13, **$p < 0.005$, paired t test, Figure 2D, left; time to max: 2.40 ± 0.40 s for Ctrl, 11.81 ± 2.46 s for SB, n = 13, **$p < 0.005$, paired t test, Figure 2D, right). In a separate set of experiments, we confirmed that cells fully recovered following washout of the drug, suggesting that this reduction did not result from photobleaching or adaptational changes (Figure S3). 5 of 13 M1 cells retained a smaller, and relatively slower, dim light-evoked response in synaptic blockers, indicating that both melanopsin and rod signaling contribute meaningfully to the dim light response of these M1 ipRGCs (Figures 2A–2C). Surprisingly, we encountered 4 M1 cells in this experiment (Figures 2A–2C, highlighted in purple in Figures 2C and 2D) that exhibited large and sustained depolarizations to dim light stimulation with 7.5 log photons cm^{-2} s^{-1}, with amplitudes that were unaffected by synaptic blocker application (Figure 2D). This indicates not only that melanopsin is contributing to the scotopic light response of some M1 ipRGCs but also that for a subset of cells, melanopsin signaling predominates even at very low light levels. Combined, these findings demonstrate an unexpectedly high sensitivity of the melanopsin response in M1 ipRGCs and suggest that most M1 ipRGCs combine synaptic and melanopsin signals at dim light intensities to drive the light response.

To specifically identify the contribution of rod versus melanopsin signaling to the M1 ipRGC dim light response, we next recorded from M1 ipRGCs in *Gnat1*$^{-/-}$ (hereafter called Gnat1KO) retinas that lack functional rod signaling or melanopsin null (*Opn4*$^{-/-}$, hereafter called MKO) retinas that lack functional melanopsin signaling (Figure 3A) and compared their dim light responses to those in wild-type (WT) retinas. Consistent with the

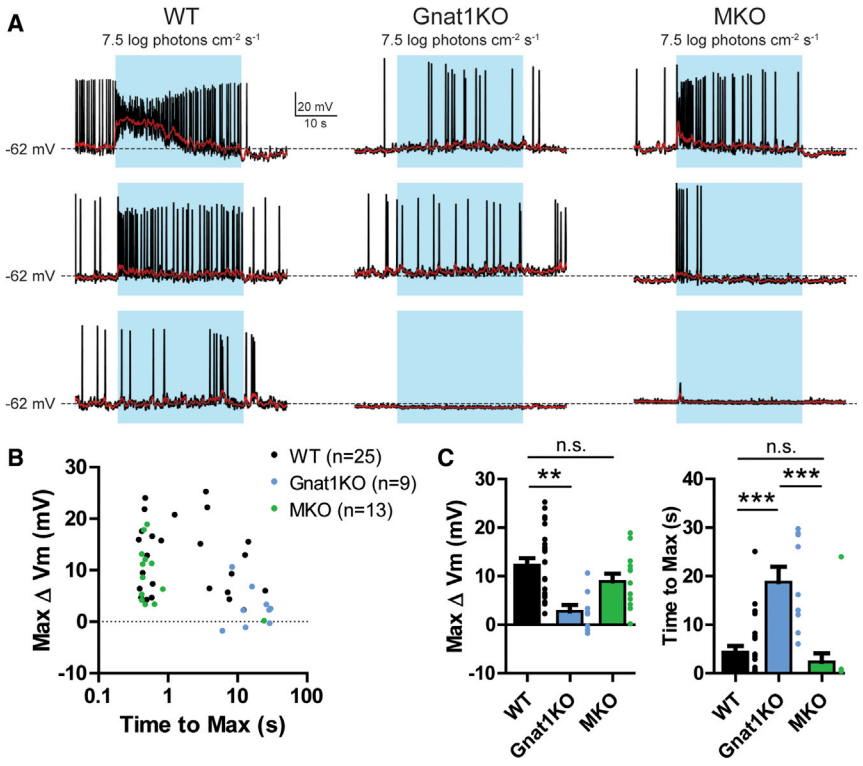

Figure 3. Synaptic Inputs to M1 ipRGCs in Dim Light Arise from the Rod Pathway

(A) Representative voltage traces of M1 ipRGCs in WT (left), Gnat1KO (middle), and MKO (right).

(B) Scatterplot of max Δ Vm versus time to max (log scale) of M1 ipRGCs in WT (black), Gnat1KO (blue), and MKO (green). M1 cells in Gnat1KO show slower responses than cells in MKO.

(C) Comparison of max Δ Vm (left) and time to max (right) of M1 ipRGCs for WT, Gnat1KO, and MKO. Bar graphs are mean ± SEM, **p < 0.005, ***p < 0.0001, one-way ANOVA post hoc Bonferroni test.

effect of synaptic blockers on the M1 cell light response in Figure 2, the M1 cells in Gnat1KO showed slower and smaller light responses (Figures 3A and 3B) than both WT and MKO. In contrast, the M1 cells in MKO showed very fast light responses (Figures 3A and 3B). When we compared the responses of WT, Gnat1KO, and MKO M1 ipRGCs, we found that the maximum depolarization in Gnat1KO M1 ipRGCs was significantly decreased compared with WT, whereas M1 ipRGCs in MKO retinas were not significantly altered (max depolarization: 12.30 ± 1.41 mV, n = 25 for WT, 2.76 ± 1.31 mV, n = 9 for Gnat1KO, 8.92 ± 1.60 mV, n = 13 for MKO, **p < 0.005, one-way ANOVA post hoc Bonferroni test; Figure 3C). The time to reach the max depolarization was also significantly increased in Gnat1KO M1 ipRGCs compared with either WT or MKO (time to max: 4.37 ± 1.23 s, n = 25 for WT, 18.77 ± 3.18 s, n = 9 for Gnat1KO, 2.31 ± 1.81 s, n = 13 for MKO, ***p < 0.0001, one-way ANOVA post hoc Bonferroni's test; Figure 3C). The difference between WT and MKO did not reach significance despite a clear shift in the kinetics of M1 ipRGCs in the MKO M1 population in Figure 3B. In MKO, we again observed multiple M1 ipRGCs that lacked an appreciable rod response (Figure 3A, bottom right, n = 3), in line with our observations in the WT M1 ipRGCs, suggesting that a subset of M1 ipRGCs simply receives little/no rod pathway input.

Dim/Scotopic Light-Evoked Response Properties Correlate with Morphological Features of M1 ipRGCs

Our physiological recordings suggest that M1 ipRGCs vary extensively in their dim light responses. We next asked whether the presence of rod input and/or the size of the dim light response correlates with the morphological features of M1 ipRGCs (Figure 4A). As a first test of this, we plotted the total dendritic length or dendritic field size against either the max depolarization or the time to max response (Figures 4B and 4C). The amplitude of M1 ipRGC depolarization evoked by a dim light stimulus showed a significant, positive correlation with total dendritic length (Pearson's r = 0.49, p < 0.005, n = 33; Figure 4B, top), though this feature did not correlate with dendritic field size (Pearson's r = 0.26, p = 0.15, n = 33; Figure 4B, bottom). In contrast, the time to reach the maximum response was significantly and negatively correlated with total dendritic length (Pearson's r = −0.51, p < 0.005, n = 33; Figure 4C, top), as well as with dendritic field size (Pearson's r = −0.41, p < 0.05, n = 33; Figure 4C, bottom).

The correlational data suggest that M1 ipRGCs with greater rod input may have larger dendritic arbors and longer total dendritic length. To test this, we next compared M1 ipRGCs that received rod input (i.e., the 8 M1 cells that showed a change in light-evoked response with synaptic blockers in Figure 2) and those that received no rod input (i.e., those with either no dim light response or a synaptic blocker-insensitive response). We found that M1 ipRGCs with confirmed rod input have significantly larger total dendritic length and dendritic fields when compared with M1 ipRGCs that lack rod input (dendritic length: 2627 ± 224.7 μm, n = 8 for rod, 1,690 ± 91.26 μm, n = 9 for no rod, **p < 0.005, unpaired t test; Figure 4D, top; dendritic field: 349.3 ± 17.6 μm, n = 8 for rod, 268.4 ± 11.46 μm, n = 9 for no rod, **p < 0.005, unpaired t test; Figure 4D, bottom).

DISCUSSION

Rod pathway input has been shown to be necessary for normal pupil constriction and normal circadian photoentrainment (Altimus et al., 2010; Keenan et al., 2016). Given that non-image-forming behaviors are thought to be mediated via M1 ipRGCs (Berson et al., 2002; Fernandez et al., 2016; Güler et al., 2008; Hattar et al., 2002, 2006), understanding the dynamics of dim light signaling within M1 ipRGCs is of paramount importance for understanding non-image-forming circuits and their retinal inputs.

In this work, we made three important discoveries. (1) The dim light response of M1 ipRGCs is quite variable, in agreement with

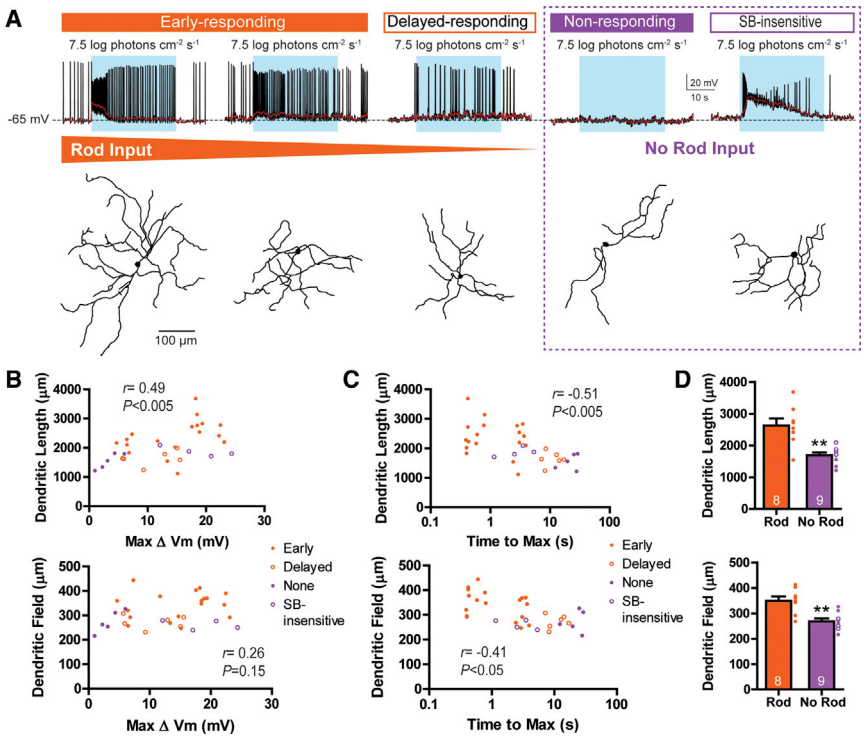

Figure 4. Dim/Scotopic Light-Evoked Response Properties Correlate with Morphological Features of M1 ipRGCs

(A) Top, representative recording examples from each of various types of M1 response arranged based on degree of rod input, which is indicated by the orange gradient. Bottom, dendrite tracing image for each recorded cell.

(B and C) Scatterplot of total dendritic length (top) and dendritic field size (bottom) versus max Δ Vm (B) or time to max (log scale) (C) for early-responding (closed orange circles, n = 18), delayed-responding (open orange circles, n = 6), non-responding (closed purple circles, n = 5), and SB-insensitive (open purple circles, n = 4) cells. The strength of max Δ Vm positively correlates with total dendritic length, whereas time to max negatively correlates with total dendritic length and dendritic field size (Pearson correlation analysis).

(D) Bar graph showing a significant difference in total dendritic length (top) and dendritic field size (bottom) between rod (orange, n = 8) and no rod (purple, n = 9). The rod group includes only M1 cells showing a decreased max Δ Vm in synaptic blockers, whereas the no rod group includes non-responding and SB-insensitive M1 cells. Bar graphs are mean ± SEM, **p < 0.005, unpaired t test.

See also Figure S4.

previous reports of M1 ipRGC variability across multiple other biophysical and morphological characteristics (Emanuel et al., 2017; Milner and Do, 2017). (2) A subset of M1 ipRGCs apparently receives no rod inputs, relaying either no information or a purely melanopsin-driven signal at low light intensities. (3) Melanopsin phototransduction is active and detectable in M1 ipRGCs at low scotopic light levels of 7.5 log photons cm^{-2} s^{-1}, adding to the growing body of evidence pointing to the exquisite sensitivity of the melanopsin system (Do et al., 2009; Sonoda et al., 2018).

Our results show that even at these very low light levels, the M1 ipRGC response is generally driven by a combination of rod inputs and melanopsin phototransduction. The M1 ipRGC dim light response was significantly reduced or eliminated with application of synaptic blockers in WT retinas (Figure 2) and was absent or reduced in Gnat1KO retinas, but it was retained in MKO retinas (Figure 3). We were particularly surprised by the robust melanopsin signaling observed at this low, scotopic light intensity, which is below the levels previously reported for melanopsin activation at 9 log photons cm^{-2} s^{-1} (Milner and Do, 2017; Sonoda et al., 2018). This result suggests that melanopsin is more sensitive than previously appreciated and contributes to dim/scotopic light signal processing in M1 ipRGCs. A previous study indicated that melanopsin integration with synaptic signals is critical to proper ipRGC function in pattern vision (Sonoda et al., 2018), and it will be important to determine whether this is also true for non-image-forming behaviors. Of note, we did not observe cells with large melanopsin responses in 9 Gnat1KO M1 ipRGCs. This could be chance, because we only recorded from 9 M1 cells in this line. It is also possible that the rod input affects proper development of the melanopsin response and that removal of this input influences ipRGC development. This will be an interesting and important avenue for future study. Fortunately, our synaptic blocker data provide a more acute test of the magnitude of rod input to M1 ipRGCs, and results from both sets of experiments suggest a substantial and variable contribution from the rod pathway to these cells.

We also observed a subset of M1 ipRGCs (4/13 cells tested) that were insensitive to synaptic blockers (Figure 2). In these cells, both the early and the delayed responses were insensitive to synaptic blockers, which indicates that their responses rely entirely on melanopsin. Their lack of synaptic input is supported by our morphological data, in which the morphological complexity of these cells is similar to that of M1 ipRGCs that lack rod inputs (Figure 4). These cells could be a subset that have melanopsin alone detecting this dim, scotopic light without rod input, as previously demonstrated for melanopsin function in bright light (Milner and Do, 2017). The robust melanopsin response we observed in some M1 ipRGCs suggests that we have not yet reached the limits of melanopsin sensitivity at low light in M1 ipRGCs.

M1 ipRGCs have been largely considered and studied as a single ipRGC population that can be distinguished from other ipRGC types based on their exclusive dendritic stratification in the OFF sublamina of the inner plexiform layer (IPL), high melanopsin expression, and high input resistance (Ecker et al., 2010; Hu et al., 2013; Schmidt and Kofuji, 2009, 2011). We find variability in the M1 ipRGC scotopic light response and a clear relationship with the presence of rod input, larger dendritic arbors, and longer total dendritic length. These features had been previously shown to be related to a handful of biophysical parameters, including synaptic amplitude and tone (Emanuel et al., 2017), though these parameters were measured at

photopic light intensity. An interesting avenue for future research will be to determine whether a larger arbor of M1 ipRGCs is simply permissive for greater connectivity with rod circuits through either the primary or the secondary rod pathways (Weng et al., 2013) or directly with rod bipolar cells (Østergaard et al., 2007) or whether there is active promotion of connectivity for a subset of M1 ipRGCs and repulsion of rod pathway input for those M1 ipRGCs receiving little/no rod input. Alternatively, it is possible that the presence of rod input during synaptogenesis in early postnatal development drives the development of larger and more complex dendritic arbors. Regardless of the mechanism, our data clearly show that the presence of rod input to M1 ipRGCs is predictive of a larger dendritic arbor and overall total dendritic length. In addition, retinal ganglion cells use different rod pathways in transmitting rod signals depending on their scotopic light sensitivities (Völgyi et al., 2004). Therefore, different subsets of M1 ipRGCs showing strong versus weak rod-driven responses could use different rod pathways. In turn, these differences could drive the diversity of dim light responses of M1 ipRGCs in dim/scotopic light.

M1 ipRGCs are required to relay dim light for normal circadian photoentrainment and the pupillary light reflex (Altimus et al., 2010; Güler et al., 2008; Keenan et al., 2016). The role for rod signaling in both of these circuits suggests that they receive input from dim-light-sensitive M1 ipRGCs. The range of dim light response characteristics suggests that as a population, M1 ipRGCs respond over a broad dynamic range, as has been proposed at higher light levels (Milner and Do, 2017). It is also possible that distinct subsets of M1 ipRGCs could signal for distinct behaviors or distinct aspects of an individual behavior. Determining the role of discrete subsets of diverse M1 ipRGCs will be a rich area for future study.

STAR★METHODS

Detailed methods are provided in the online version of this paper and include the following:

- KEY RESOURCES TABLE
- LEAD CONTACT AND MATERIALS AVAILABILITY
- EXPERIMENTAL MODEL AND SUBJECT DETAILS
- METHOD DETAILS
  - *Ex vivo* retina preparation
  - Electrophysiology
  - Immunohistochemistry
  - Confocal imaging and morphological analysis
- QUANTIFICATION AND STATISTICAL ANALYSIS
- DATA AND CODE AVAILABILITY

SUPPLEMENTAL INFORMATION

Supplemental Information can be found online at https://doi.org/10.1016/j.celrep.2019.11.024.

ACKNOWLEDGMENTS

We thank members of the Schmidt lab for helpful comments on the manuscript and Dr. Samer Hattar for the gift of *Opn4*^{LacZ} and *Gnat1*$^{-/-}$ mice. This work was funded by NIH grant 1DP2EY022584, a Sloan Research Fellowship in Neuroscience, and a Klingenstein-Simons Fellowship in the Neurosciences to T.M.S. and NIH grant F31 EY030360 to T.S.

AUTHOR CONTRIBUTIONS

S.K.L. and T.M.S. designed experiments and wrote the paper. S.K.L. and T.S. performed experiments and analysis.

DECLARATION OF INTERESTS

The authors declare no competing interests.

Received: March 21, 2019
Revised: September 4, 2019
Accepted: November 6, 2019
Published: December 10, 2019

REFERENCES

Altimus, C.M., Güler, A.D., Alam, N.M., Arman, A.C., Prusky, G.T., Sampath, A.P., and Hattar, S. (2010). Rod photoreceptors drive circadian photoentrainment across a wide range of light intensities. Nat. Neurosci. *13*, 1107–1112.

Berson, D.M., Dunn, F.A., and Takao, M. (2002). Phototransduction by retinal ganglion cells that set the circadian clock. Science *295*, 1070–1073.

Calvert, P.D., Krasnoperova, N.V., Lyubarsky, A.L., Isayama, T., Nicoló, M., Kosaras, B., Wong, G., Gannon, K.S., Margolskee, R.F., Sidman, R.L., et al. (2000). Phototransduction in transgenic mice after targeted deletion of the rod transducin alpha -subunit. Proc. Natl. Acad. Sci. USA *97*, 13913–13918.

Do, M.T., Kang, S.H., Xue, T., Zhong, H., Liao, H.W., Bergles, D.E., and Yau, K.W. (2009). Photon capture and signalling by melanopsin retinal ganglion cells. Nature *457*, 281–287.

Ecker, J.L., Dumitrescu, O.N., Wong, K.Y., Alam, N.M., Chen, S.K., LeGates, T., Renna, J.M., Prusky, G.T., Berson, D.M., and Hattar, S. (2010). Melanopsin-expressing retinal ganglion-cell photoreceptors: cellular diversity and role in pattern vision. Neuron *67*, 49–60.

Emanuel, A.J., Kapur, K., and Do, M.T.H. (2017). Biophysical Variation within the M1 Type of Ganglion Cell Photoreceptor. Cell Rep. *21*, 1048–1062.

Estevez, M.E., Fogerson, P.M., Ilardi, M.C., Borghuis, B.G., Chan, E., Weng, S., Auferkorte, O.N., Demb, J.B., and Berson, D.M. (2012). Form and function of the M4 cell, an intrinsically photosensitive retinal ganglion cell type contributing to geniculocortical vision. J. Neurosci. *32*, 13608–13620.

Fernandez, D.C., Chang, Y.T., Hattar, S., and Chen, S.K. (2016). Architecture of retinal projections to the central circadian pacemaker. Proc. Natl. Acad. Sci. USA *113*, 6047–6052.

Güler, A.D., Ecker, J.L., Lall, G.S., Haq, S., Altimus, C.M., Liao, H.W., Barnard, A.R., Cahill, H., Badea, T.C., Zhao, H., et al. (2008). Melanopsin cells are the principal conduits for rod-cone input to non-image-forming vision. Nature *453*, 102–105.

Hattar, S., Liao, H.W., Takao, M., Berson, D.M., and Yau, K.W. (2002). Melanopsin-containing retinal ganglion cells: architecture, projections, and intrinsic photosensitivity. Science *295*, 1065–1070.

Hattar, S., Kumar, M., Park, A., Tong, P., Tung, J., Yau, K.W., and Berson, D.M. (2006). Central projections of melanopsin-expressing retinal ganglion cells in the mouse. J. Comp. Neurol. *497*, 326–349.

Hu, C., Hill, D.D., and Wong, K.Y. (2013). Intrinsic physiological properties of the five types of mouse ganglion-cell photoreceptors. J. Neurophysiol. *109*, 1876–1889.

Keenan, W.T., Rupp, A.C., Ross, R.A., Somasundaram, P., Hiriyanna, S., Wu, Z., Badea, T.C., Robinson, P.R., Lowell, B.B., and Hattar, S.S. (2016). A visual circuit uses complementary mechanisms to support transient and sustained pupil constriction. eLife *5*, e15392.

Lee, S.K., and Schmidt, T.M. (2018). Morphological Identification of Melanopsin-Expressing Retinal Ganglion Cell Subtypes in Mice. Methods Mol. Biol. *1753*, 275–287.

Li, J.Y., and Schmidt, T.M. (2018). Divergent projection patterns of M1 ipRGC subtypes. J. Comp. Neurol. *526*, 2010–2018.

Lucas, R.J., Hattar, S., Takao, M., Berson, D.M., Foster, R.G., and Yau, K.W. (2003). Diminished pupillary light reflex at high irradiances in melanopsin-knockout mice. Science *299*, 245–247.

Milner, E.S., and Do, M.T.H. (2017). A Population Representation of Absolute Light Intensity in the Mammalian Retina. Cell *171*, 865–876.

Østergaard, J., Hannibal, J., and Fahrenkrug, J. (2007). Synaptic contact between melanopsin-containing retinal ganglion cells and rod bipolar cells. Invest. Ophthalmol. Vis. Sci. *48*, 3812–3820.

Panda, S., Provencio, I., Tu, D.C., Pires, S.S., Rollag, M.D., Castrucci, A.M., Pletcher, M.T., Sato, T.K., Wiltshire, T., Andahazy, M., et al. (2003). Melanopsin is required for non-image-forming photic responses in blind mice. Science *301*, 525–527.

Schindelin, J., Arganda-Carreras, I., Frise, E., Kaynig, V., Longair, M., Pietzsch, T., Preibisch, S., Rueden, C., Saalfeld, S., Schmid, B., et al. (2012). Fiji: an open-source platform for biological-image analysis. Nat. Methods *9*, 676–682.

Schmidt, T.M., and Kofuji, P. (2009). Functional and morphological differences among intrinsically photosensitive retinal ganglion cells. J. Neurosci. *29*, 476–482.

Schmidt, T.M., and Kofuji, P. (2011). Structure and function of bistratified intrinsically photosensitive retinal ganglion cells in the mouse. J. Comp. Neurol. *519*, 1492–1504.

Schmidt, T.M., Taniguchi, K., and Kofuji, P. (2008). Intrinsic and extrinsic light responses in melanopsin-expressing ganglion cells during mouse development. J. Neurophysiol. *100*, 371–384.

Sonoda, T., Lee, S.K., Birnbaumer, L., and Schmidt, T.M. (2018). Melanopsin Phototransduction Is Repurposed by ipRGC Subtypes to Shape the Function of Distinct Visual Circuits. Neuron *99*, 754–767.

Völgyi, B., Deans, M.R., Paul, D.L., and Bloomfield, S.A. (2004). Convergence and segregation of the multiple rod pathways in mammalian retina. J. Neurosci. *24*, 11182–11192.

Weng, S., Estevez, M.E., and Berson, D.M. (2013). Mouse ganglion-cell photoreceptors are driven by the most sensitive rod pathway and by both types of cones. PLoS ONE *8*, e66480.

Zhao, X., Stafford, B.K., Godin, A.L., King, W.M., and Wong, K.Y. (2014). Photoresponse diversity among the five types of intrinsically photosensitive retinal ganglion cells. J. Physiol. *592*, 1619–1636.

STAR★METHODS

KEY RESOURCES TABLE

REAGENT or RESOURCE	SOURCE	IDENTIFIER
Antibodies		
Rabbit polyclonal anti-GFP	ThermoFisher	Cat# A-11122, RRID:AB_221569
Donkey anti-rabbit IgG (H+L) secondary antibody, Alexa Fluor 488	ThermoFisher	Cat#A21206, RRID:AB_141708
Streptavidin, Alexa Fluor 546-conjugated	ThermoFisher	Cat#S11225, RRID:AB_2532130
Chemicals, Peptides, and Recombinant Proteins		
Neurobiotin Tracer	Vector Laboratories	Cat#SP-1120-20
Hydrazide, Alexa Fluor 594 conjugated	ThermoFisher	Cat#A10438
DNQX	Tocris Bioscience	Cat#0189
L-AP4	Tocris Bioscience	Cat#0103
Experimental Models: Organisms/Strains		
Mouse: *Opn4-GFP* (BAC transgenic reporter)	Schmidt et al., 2008	N/A
Mouse: *Opn4*$^{-/-}$	Hattar et al., 2002	RRID: MGI:6192520
Mouse: *Gnat1*$^{-/-}$	Calvert et al., 2000	N/A
Software and Algorithms		
MATLAB (R2015a)	MathWorks	https://www.mathworks.com/products/matlab.html; RRID: SCR_001622
pClamp 10.7	Molecular Devices	https://www.moleculardevices.com/#gref; RRID: SCR_011323
Graphpad Prism 6	GraphPad	https://www.graphpad.com/; RRID: SCR_002798
Fiji	Schindelin et al., 2012	http://fiji.sc/; RRID:SCR_002285

LEAD CONTACT AND MATERIALS AVAILABILITY

Further information and requests for resources and reagents should be directed to and will be fulfilled by the Lead Contact, Tiffany M. Schmidt (tiffany.schmidt@northwestern.edu). This study did not generate new or unique reagents.

EXPERIMENTAL MODEL AND SUBJECT DETAILS

All experimental protocols were approved by the Northwestern University Animal Care and Use Committee. 1∼2 month-old male and female mice were used on a mixed Bl6/129 background. For M1 ipRGC recordings, the *Opn4-GFP* mouse line (Schmidt et al., 2008) crossed with WT, *Opn4*$^{-/-}$ (Hattar et al., 2002), or *Gnat1*$^{-/-}$ (Calvert et al., 2000) was used.

METHOD DETAILS

Ex vivo retina preparation

Animals were dark-adapted overnight, anesthetized by CO_2 and then sacrificed by cervical dislocation. Eyes were enucleated and retinas were dissected in oxygenated (95% O_2-5% CO_2) Ames' medium (Sigma) under dim red light. Retinas were cut in half and incubated in oxygenated Ames' medium at 26 C for at least 30 min before use.

Electrophysiology

Retinas were mounted with ganglion cell layer up on a recording chamber and secured using a harp with nylon mesh (Warner Instruments). The chamber was placed on the stage of a customized electrophysiology rig (Scientifica) and the retina was perfused with oxygenated Ames' medium (4-5 mL/min) and maintained at 25-26 C using a temperature controller (Warner Instruments).

The ganglion cell layer of the retina is visualized using infrared differential interference contrast optics (infrared DIC, 940 nm, Figure S1A). GFP-labeled ipRGCs (M1-M3) were randomly targeted based on their somatic GFP signals visualized by a 2-photon laser excitation (910 nm, 9 μW, < 10 s, Spectra Physics). M1 ipRGC identity was confirmed by intracellular dye (Neurobiotin) filling and post hoc immunohistochemistry and confocal microscopy following recording based on the presence of dendrites exclusively stratifying in the OFF-sublamina of the inner plexiform layer (IPL) (Figure S1B) (Schmidt and Kofuji, 2009, 2011).

Whole cell recordings were performed using a Multiclamp 700B amplifier (Molecular devices) using fire-polished borosilicate pipettes (4-7 MΩ; Sutter Instruments). All current and voltage traces were sampled at 10 kHz, low-pass filtered at 2 kHz and acquired using a Digidata 1550B and pClamp 10 software (Molecular devices). All recordings are made in oxygenated Ames' medium which is buffered with 23 mM sodium bicarbonate. For experiments with synaptic blocker cocktail, 100 μM 6,7-Dinitroquinoxaline-2,3-dione (DNQX; selective AMPA/kainate receptor antagonist; Tocris), 20 μM L-2-amino-4-phosphonobutylic acid (L-AP4; selective group III metabotropic glutamate receptor agonist; Tocris) were added to Ames' medium. Internal pipette solution included (in mM) 125 K-gluconate, 2 $CaCl_2$, 2 $MgCl_2$. 10 EGTA, 10 HEPES, 2 Na_2-ATP, 0.5 Na-GTP. 0.3% Neurobiotin (Vector Laboratories) and Alexa Fluor 594 conjugated-hydrazide (10 μM, Thermo) were added to internal solution prior to recording.

For light response experiments, recordings were made in current clamp mode. In our recordings from WT retinas, resting membrane potential of M1 ipRGCs was −62 mV on average. For M1 ipRGCs showing a hyperpolarized (< −65 mV) or depolarized (> −59 mV) resting membrane potential (Figure 1) or when the membrane potential was changed after application of synaptic blockers (Figure 2), current was injected to adjust membrane potential to near −62 mV. In this case, cells were bridge balanced.

The blue LED light (~480 nm) was used to deliver light stimuli to the retina through a 60X water-immersion objective. The light intensity was adjusted using neutral density filters (Thor Labs). Before recording, retinas were dark-adapted for at least 10 min.

Immunohistochemistry

After recording, retinas were fixed in 4% paraformaldehyde (Electron Microscopy Sciences) in 1X PBS for 30 min-1 hr at room temperature (RT) and then washed 3X20 min in 1X PBS. Retinas were then placed in blocking solution containing 5% donkey serum (Sigma) in 0.3% Triton-X PBS (PBS_{TX}) for 1 hr at RT. Then, retinas were incubated in primary antibody solution containing rabbit anti-GFP (1:1000, Thermo) in 2% donkey PBS_{TX} for 3 days at 4 C and washed for 3X20 min in 1X PBS, and then incubated in secondary antibody solution including Alexa Fluor 488 donkey anti-rabbit (1:1000, Thermo) in 2% donkey PBS_{TX} for 2 hrs at RT. Alexa Fluor 546-conjugated streptavidin (1:500, Thermo) was included in both primary and secondary antibody solution. Retinas were washed for 3X20 min in 1X PBS and then mounted using Fluoromount aqueous mounting medium (Sigma).

Confocal imaging and morphological analysis

The images for immunostained retinas were acquired using confocal laser scanning microscope (Leica DM5500 SPE, Leica microsystems). A 40X oil-immersion objective was used for confocal scanning because some of M1 ipRGCs' dendrites are too tiny to be visible in lower resolutions (Lee and Schmidt, 2018). Since one image is not able to include whole dendrites of M1 ipRGCs, multiple stacked images (spanning from the ganglion cell layer to inner nuclear layer) were taken in order to cover all dendrites of the cell and then stitched manually in Adobe Photoshop CC (Adobe systems).

QUANTIFICATION AND STATISTICAL ANALYSIS

All reported voltages are corrected for liquid junction potential (−14 mV). All voltage traces and spike frequency plots were made using MATLAB software (Mathworks). To measure membrane potential, voltage traces were filtered using a 0.5 s moving average. "Maximum depolarization (Max Δ Vm)" and "time to max" was measured as voltage value and time at which membrane potential reached maximum during a 30 s light stimulation. To measure spike frequency, voltage traces are baseline adjusted manually to 0 mV using Clampfit (Molecular devices) and action potentials (amplitude > 20 mV) were detected and counted using a threshold search event detection tool. The spike frequency is plotted as the number of spikes per 1 s bin.

Morphological analysis was performed using Fiji software (Schindelin et al., 2012). Dendrites of the cell were traced using NeuronJ plugin and measured total dendritic length. Dendritic field size was estimated by taking the area of a convex polygon connected the terminating points of the outmost dendrites (blue points in Figure S4) and, in case of that dendritic processes were found beyond the range of the polygon, the outmost point of the dendritic processes (Magenta points in Figure S4) in a two-dimensional tracing of a given cell (Ecker et al., 2010; Estevez et al., 2012; Schmidt and Kofuji, 2011; Schmidt et al., 2008). The dendritic field size was expressed as a diameter in assumption that the polygon area is a circle.

Graphing and statistical analysis was performed using GraphPad Prism 6 software. All bar graphs represent the means ± SEMs. For comparison, unpaired (Figures 1E and 4D) or paired (Figure 2D) two-tailed t test and one-way ANOVA test (Figure 3C) was used. For correlation, Pearson correlation test was used. Significance was set when $p < 0.05$. n represents the number of cells tested.

DATA AND CODE AVAILABILITY

Requests for custom scripts and raw data can be directed to the Lead Contact, Tiffany M. Schmidt (tiffany.schmidt@northwestern.edu).